Efficient, Accurate and Robust Approximation of Clothoids for Path Smoothing

Yong Chen, Yiyu Cai, and Daniel Thalmann

***Abstract*—We present a smooth approximation approach for general clothoids with arbitrary parameters to achieve 3rd order geometric continuity. A subset of clothoids with specific winding angle constraints referred to as elementary clothoids are approximated using quintic Bézier curves. Optimal values of shape parameters are obtained in a deterministic way by minimizing the error of curvature profiles between the clothoid and the Bézier curve. Then a basic clothoid defined in the first quadrant can be conveniently computed and stored in a lookup table, which significantly speeds up the approximation process of general clothoids with any prescribed parameters via appropriate geometric transformations. A comprehensive error analysis presented verifies that the approach guarantees divergence-free and robust results with high accuracy.**

***Index Terms*—Clothoid approximation, geometric continuity, numerical optimization, path smoothing.**

I. Introduction

FINDING a feasible path is non-trivial for wheeled robots especially those under differential constraints. A practical planner should satisfy certain conditions limited by the kinematic and dynamic properties of the robot while avoid obstacles in the environment [1]. A common way of achieving this is to compute a series of configurations and jointing them with continuous oriented curves. Valid curves should satisfy the upper-bounded curvature constraints imposed by the kinematic properties of the robot when rolling without slipping is assumed [2]. The optimal solution connecting two distinct configurations can be obtained by applying Pontryagin's Maximum Principle on Dubins model, and the extremal path is composed of line segments and arcs of clothoids [3]. Additionally, due to the linear curvature property, clothoids are easy to follow and thus widely used as transition curves for path smoothing applications [4]. As an example, a steering method made up of a cltohoid pair and a circular arc is presented in [5] to form a smooth path with upper-bounded curvature.

Despite such attractive properties, clothoids are difficult to be implemented in real time applications since they are defined by Fresnel integrals which have no closed form. Consequently, various curves have been proposed as alternative solutions for smooth path planning, such as Bézier curves of different degrees in [6], [7] and [8], Fermat's spiral [9], Pythagorean-hodograph curve [10], etc. To achieve monotonic curvature profiles or equivalent quality as clothoid paths, a number of methods have been proposed to compute or approximate clothoids, and generally these approaches fall into two categories. The first group of methods attempt to compute the clothoid coordinates in a pointwise manner. For example, [11] takes discrete samples from the clothoid and interpolating these points with circular arcs, and the accuracy improves as the sampling interval becomes narrower. On the other hand, clothoid coordinates can be directly calculated by computing Fresnel integrals numerically in [12] and [13]. The major drawback of these methods is that the geometric information is lost such as curvature and sharpness, which, however, are of great importance to path planning and smoothing applications. Instead of point-by-point approaches, another group of methods resort to smooth approximation using continuous curves with simpler forms, whose geometric information can be retrieved handily. In this category polynomials including Bézier curves are appropriate candidates and a wide variety of methods has been extensively studied. A typical example is the Bézier curve approximation using Taylor expansion [14], but the resulting Bézier curve can be of high degree which is not suitable for real time applications. Instead, s-power series [15] are employed to construct an order-k Hermite interpolant, which generates a C^k continuous Hermitian spline [16]. As an instance of generalized Cornu spiral (GCS), a clothoid can also be approximated based on curvature profiles, and the obtained quintic Bézier curve manages to preserve G^2 continuity at end points through numerical optimization [17]. Furthermore, G^3 condition can be achieved in a similar manner with improved objective functions presented in [18] and [19]. To avoid numerical search which is computationally intensive and unstable in certain cases, a G^{2+} deterministic approximation method is proposed in [20] which introduces linear interpolations to address the divergent regions. Although these methods generate acceptable Bézier curve approximations with sufficient accuracy, they suffer from the same drawback that the winding angle of targeted clothoid has to be defined within $[0, \frac{\pi}{2}]$. Additionally a clothoid of non-unit length is required to be normalized, and hence only clothoids whose winding angles fall in the allowed range after normalization can be handled by these approaches and they are not applicable to a generic clothoid with arbitrary parameters.

In this paper, we propose a generic Bézier curve approximation method which in theory can deal with any types of clothoids. Since commonly used approaches only focus on unit-length clothoid, reparameterizing with respect to arc length, scaling and rescaling are required in most scenarios. However, these redundant procedures can be avoided by directly targeting at elementary clothoids with arbitrary positive arc length. Accordingly we apply G^3 condition to the quintic Bézier curve and the clothoid to obtain a Bézier representation with two free shape parameters. To determine the optimal values for these parameters, a reasonable approximation with

regard to the curve length is applied and the assumption is validated through numerical optimizations and error analysis. Also, we resolve the divergence problem by restricting arc length of the elementary clothoid within a safe region. Thus the algorithm used is highly robust and always able to produce reasonable results in a deterministic way. Next a lookup table to efficiently compute a basic clothoid is built on the grounds that it can be regarded as a composition of infinite pieces of elementary clothoids. Finally due to the fact that a general clothoid can be represented with a piece of curve located in the lookup table via appropriate geometric transformation, any clothoid with arbitrary parameters can be approximated with G^3 continuity. The approximation error is analyzed numerically and the accuracy is adjustable by choosing different winding angle parameters. Finally both unit-length and non-unit length approximation examples are demonstrated using proposed approach and comparisons are made against several other algorithms. Also we apply our method to a practical path smoothing problem and demonstrate that the resulting path achieves better quality than other smoothing methods from perspective of path length and curvature maxima.

The rest of this paper is organized as follows. Section II describes the approximation procedures of an elementary clothoid with G^3 continuity. The results are used to compose a basic clothoid serving as a lookup table with error analysis in Section III. In Section IV, approximation of a general clothoid with arbitrary parameters is presented. Lastly, the effectiveness of the proposed method is tested and compared with other algorithms in Section V.

II. Elementary Clothoid Approximation

A. Clothoid

Clothoid is also referred to as Euler spiral or Cornu spiral and its curvature $\kappa(s)$ can be expressed as a linear function of its curve length s:

$$\kappa(s) = \kappa_0 + \sigma s, \quad \kappa_0,\, \sigma \in \mathbb{R}, \tag{1}$$

where σ is the sharpness of the clothoid and κ_0 is the initial curvature as $s = 0$. The tangent or winding angle $\theta(s)$ with respect to its curve length s is

$$\theta(s) = \theta_0 + \kappa_0 s + \frac{\sigma s^2}{2}, \quad \theta_0,\, \kappa_0,\, \sigma \in \mathbb{R}, \tag{2}$$

where θ_0 is the initial angle when $s = 0$. Thus, a general clothoid can be expressed in parametric form as in [21]:

$$\mathbf{F}(s) = \begin{pmatrix} x_0 + \int_0^s \cos\left(\theta_0 + \kappa_0 u + \frac{\sigma u^2}{2}\right) du \\ y_0 + \int_0^s \sin\left(\theta_0 + \kappa_0 u + \frac{\sigma u^2}{2}\right) du \end{pmatrix}. \tag{3}$$

Based on (3) we can define a piece of elemental clothoid denoted by $\mathbf{F}_\varepsilon(s)$ with a positive sharpness $\sigma_\varepsilon > 0$. Furthermore, it is restricted to the first quadrant, thus $s \in [0, \infty)$ and initial conditions are specified as $(x_0, y_0) = (0, 0)$, $\theta_0 = 0$ and $\kappa_0 \geqslant 0$:

$$\mathbf{F}_\varepsilon(s) = \sqrt{\frac{\pi}{\sigma_e}}\mathbf{R}\left(-\frac{\kappa_0^2}{2\sigma_\varepsilon}\right)\begin{pmatrix}\delta_c(s)\\ \delta_s(s)\end{pmatrix}, \tag{4}$$

where $\delta_c(s) = C(\frac{\sigma_\varepsilon s+\kappa_0}{\sqrt{\pi\sigma_\varepsilon}}) - C(\frac{\kappa_0}{\sqrt{\pi\sigma_\varepsilon}})$, $\delta_s(s) = S(\frac{\sigma_\varepsilon s+\kappa_0}{\sqrt{\pi\sigma_\varepsilon}}) - S(\frac{\kappa_0}{\sqrt{\pi\sigma_\varepsilon}})$. Here, $\mathbf{R}(\theta)$ is the planar rotation matrix

$$\mathbf{R}(\theta) = \begin{pmatrix}\cos(\theta) & -\sin(\theta)\\ \sin(\theta) & \cos(\theta)\end{pmatrix}, \tag{5}$$

and $C(t)$ and $S(t)$ are a pair of nonnegative functions named Fresnel integrals [22]:

$$C(t) = \int_0^t \cos\left(\frac{\pi u^2}{2}\right) du,\; S(t) = \int_0^t \sin\left(\frac{\pi u^2}{2}\right) du. \tag{6}$$

B. Quintic Bézier Curve

Assuming that the quintic Bézier curve

$$\mathbf{B}_\varepsilon(t) = \sum_{i=0}^{5}\binom{5}{i}(1-t)^{5-i}t^i\mathbf{V}_i, \quad t \in [0,1]. \tag{7}$$

is a feasible approximation to a piece of elementary clothoid curve $\mathbf{F}_\varepsilon(s)$. Let u_b and u denote the total length of $\mathbf{B}_\varepsilon(t)$ and $\mathbf{F}_\varepsilon(s)$ respectively. Without loss of generality, in addition to the G^2 condition in [17] we need to apply the following constraint to $\mathbf{B}_\varepsilon(t)$ at two ends to achieve G^3 continuity:

$$\begin{aligned}\kappa_b'(s)|_{s=0} &= \kappa_c'(s)|_{s=0},\\ \kappa_b'(s)|_{s=u_b} &= \kappa_c'(s)|_{s=u},\end{aligned} \tag{8}$$

where κ_b, κ_c represent the curvature profiles of $\mathbf{B}_\varepsilon(t)$ and $\mathbf{F}_\varepsilon(s)$ respectively. Considering the inconvenience of representing the curvature profile of a quintic Bézier curve with regard to arc length analytically as required by (8), an equivalent condition using Beta-constraints with shape parameters [23] is adopted instead. Accordingly, the control points $\mathbf{V}_i$ $(i = 0, 1, 2, \ldots, 5)$ are expressed as

$$\begin{pmatrix}\mathbf{V}_0\\ \mathbf{V}_1\\ \mathbf{V}_2\\ \mathbf{V}_3\\ \mathbf{V}_4\\ \mathbf{V}_5\end{pmatrix} = \begin{pmatrix}\mathbf{F}_\varepsilon(0)\\ \frac{\beta_1}{5}\mathbf{F}_\varepsilon'(0) + \mathbf{F}_\varepsilon(0)\\ \frac{\beta_1^2}{20}\mathbf{F}_\varepsilon''(0) + \frac{8\beta_1+\beta_2}{20}\mathbf{F}_\varepsilon'(0) + \mathbf{F}_\varepsilon(0)\\ \frac{\gamma_1^2}{20}\mathbf{F}_\varepsilon''(u) + \frac{\gamma_2-8\gamma_1}{20}\mathbf{F}_\varepsilon'(u) + \mathbf{F}_\varepsilon(u)\\ -\frac{\gamma_1}{5}\mathbf{F}_\varepsilon'(u) + \mathbf{F}_\varepsilon(u)\\ \mathbf{F}_\varepsilon(u)\end{pmatrix} \tag{9}$$

where shape parameters β_2 and γ_2 are indeed dependent on the other two free parameters $\beta_1 > 0$ and $\gamma_1 > 0$, and likewise can be calculated as in [20]:

$$\beta_2(\beta_1,\gamma_1) = \frac{B(\beta_1,\gamma_1)}{D(\beta_1,\gamma_1)}, \quad \gamma_2(\beta_1,\gamma_1) = \frac{G(\beta_1,\gamma_1)}{D(\beta_1,\gamma_1)}. \tag{10}$$

The common denominator function $D(\beta_1, \gamma_1)$ can be expressed as

$$D(\beta_1,\gamma_1) = \beta_1\gamma_1\kappa_0\kappa_1 - \sin^2(\theta), \tag{11}$$

where $\kappa_1 = \kappa_0 + \sigma_\varepsilon u$ is the final curvature at endpoint as $s = u$.

C. Approximation

To guarantee the approximation error is within acceptable tolerance, the winding angle θ is restricted to

$$0 < \theta \leqslant \frac{\pi}{2}. \tag{12}$$

Taking a piece of normalized clothoid $\mathbf{F}_\varepsilon(s)$ with $s \in [0,1]$ and $\kappa_0 = 0$ as an example, its sharpness σ_ε is limited to $(0, \pi]$ by applying (12). Although it seems to be a limitation here, later on we will show that a general clothoid can be approximated free of such constraints. To measure the approximation quality, the error $\epsilon_\kappa(s)$ is defined as a function of arc length parameter s by combining the expressions of absolute difference and relative difference [18]. To compute $\epsilon_\kappa(s)$, the curvatures of both the clothoid and corresponding Bézier curve have to be represented with arc length parameter as $\kappa_c(s)$ and $\kappa_b(s)$ respectively. Therefore, extra procedures need to be taken to re-parameterize Bézier curve w.r.t. arc length s, and this can be achieved by numerical approximation [24] or iterative sampling [25]. The maxima of $\epsilon_\kappa(s)$ over the entire domain $[0, u]$

$$\epsilon_\kappa = \max_{s\in[0,u]} \epsilon_\kappa(s) = \max_{s\in[0,u]} \frac{|\kappa_b(s) - \kappa_c(s)|}{\max\{|\kappa_c(s)|, 1\}} \tag{13}$$

is used to quantify the approximation error. The approximated curve is acceptable if $\epsilon_\kappa \leqslant \mu$, and a tolerance of $\mu = 0.05$ can be adopted [26] in most cases.

As in [20], by introducing a new parameter $k = \kappa_0 - \kappa_1$ and assuming β_1 and γ_1 are relatively stable as k varies, we can represent sharpness and curvature values with regard to winding angle θ and parameter k:

$$\begin{aligned} \sigma_\varepsilon &= -\frac{k}{u}, \\ \kappa_0 &= \frac{k}{2} + \frac{\theta}{u}, \\ \kappa_1 &= -\frac{k}{2} + \frac{\theta}{u}, \end{aligned} \tag{14}$$

where $u > 0$ is the total arc length. Substituting (9) and (10) into (7) successively, the desired quintic Bézier curve $\mathbf{B}_\varepsilon(t)$ can be expressed as a function of shape parameter β_1 and γ_1. Then by applying the relationship (14) to obtained Bézier curve and elementary clothoid (4), they can be formulated as $\tilde{\mathbf{B}}_\varepsilon(s, u, k, \theta, \beta_1, \gamma_1)$ and $\mathbf{F}_\varepsilon(s, u, k, \theta)$ separately after reparameterization w.r.t. arc length. In such a way the maximum error of curvature (13) actually can be expressed as $\epsilon_\kappa(\beta_1, \gamma_1)$. By solving for the constrained optimization problem

$$\begin{aligned} \min \quad & \epsilon_\kappa(\beta_1, \gamma_1) \\ \text{s.t.} \quad & \beta_1 > 0, \gamma_1 > 0 \end{aligned} \tag{15}$$

the most desirable values of two free variables, i.e., β_1 and γ_1, can be determined. Accordingly, the optimal quintic Bézier curve among all the candidates satisfying G^3 continuity condition can be computed.

Since there is no exact closed expression of $\kappa_b(s)$ in (13) , here for simplicity we use the Hermite interpolation based method [24] to approximate the inverse of arc length function of $\mathbf{B}_\varepsilon(t)$. The value of a cubic interpolation function is used to obtain parameter t at given normalized arc length $\frac{s}{u} \in [0,1]$, and the accuracy can be further improved by approximating the target curve with multiple segments according to Simpson' rule and reparameterizing each segment respectively. With values of $\kappa_b(s)$ and $\kappa_c(s)$ computed subsequently, the minima of $\epsilon_\kappa(\beta_1, \gamma_1)$ is expected to be acquired. In [20] an analysis of a set of generalized Cornu spirals with unit arc length, i.e., $u = 1$, suggests that $(\beta_1, \gamma_1) = (1, 1)$ is an effective approximation of the solution to problem (15) for clothoid curves. From (9) we can see that β_1 and γ_1 are closely related to the edge lengths of the control polygon: $\|\mathbf{V}_1 - \mathbf{V}_0\| = \frac{\beta_1}{5}$ and $\|\mathbf{V}_5 - \mathbf{V}_4\| = \frac{\gamma_1}{5}$, which increase linearly with the total arc length u of the clothoid. Consequently, it is reasonable to assume that $(\beta_1, \gamma_1) = (u, u)$ is the optimal solution for clothoids of non-unit length.

A numerical optimization procedure to solve for (15) is implemented to verify our assumption by performing a search starting at the initial position $(\beta_1, \gamma_1) = (u, u)$. The objective function $\epsilon_\kappa(\beta_1, \gamma_1)$ is evaluated by calculating differences of corresponding values at uniformly sampled positions of two parameterized curves, and its gradient can be estimated using finite differences due to lack of derivative information, or adopting derivative free optimization algorithms like Nelder-Mead method [27] instead. Fig. 1 shows different $\epsilon_\kappa(\beta_1, \gamma_1)$ values computed over region $[0, 10\,u] \times [0, 10\,u]$ and totally 10 points are sampled uniformly on each curve. The arc length u is set to 0.1, 1.0, and 10.0 respectively as the winding angle changes from $\frac{\pi}{4}$ to $\frac{\pi}{42}$. The black points around (u, u) shown in the figure represent coordinates evaluated during the search process with a ring of minima $|\epsilon_\kappa - \min \epsilon_\kappa(\beta_1, \gamma_1)| \leqslant 0.05$. Other numerical evaluations for different combinations of u and θ values yield consistent results that the distributions of $\epsilon_\kappa(\beta_1, \gamma_1)$ have similar patterns while the minima always appears around (u, u). This confirms that the optimal values of β_1 and γ_1 can be regarded as independent of winding angle. To further elaborate the relationship among shape parameters (β_1, γ_1), arc length u and k, a numerical search across different combinations is performed. The optimal values of β_1 and γ_1 are represented in the form of $\beta_1(u, k, \theta)$ and $\gamma_1(u, k, \theta)$ respectively as shown in Fig. 2. It can be clearly seen that obtained β_1 and γ_1 are approximately proportional to arc length u and the effects from both winding angle θ and k can be neglected. This is consistent with our assumption that

$$\beta_1(u, k, \theta) \doteq u, \quad \gamma_1(u, k, \theta) \doteq u \tag{16}$$

can be considered as the optimal position. However, another problem occurs when we adhere to G^3 continuity since such values of β_2 and γ_2 do not always exist by taking a close look at (10). More specifically, by substituting (14) into (11), a divergence will occur when $D(\beta_1, \gamma_1)$ approaches zero if

$$k = \pm k_d = \pm 2\sqrt{\frac{\theta^2}{u^2} - \frac{\sin^2(\theta)}{\beta_1 \gamma_1}}. \tag{17}$$

The divergence problem is illustrated in Fig. 3. In this case, the values of β_2 and γ_2 have infinite discontinuities at $k = \pm k_d$ and extra compromised procedures are required to obtain a continuous and smooth curve. In [20], linear approximations of β_2 and γ_2 are made in region $(-2\,k_d, 2\,k_d)$ to smoothen

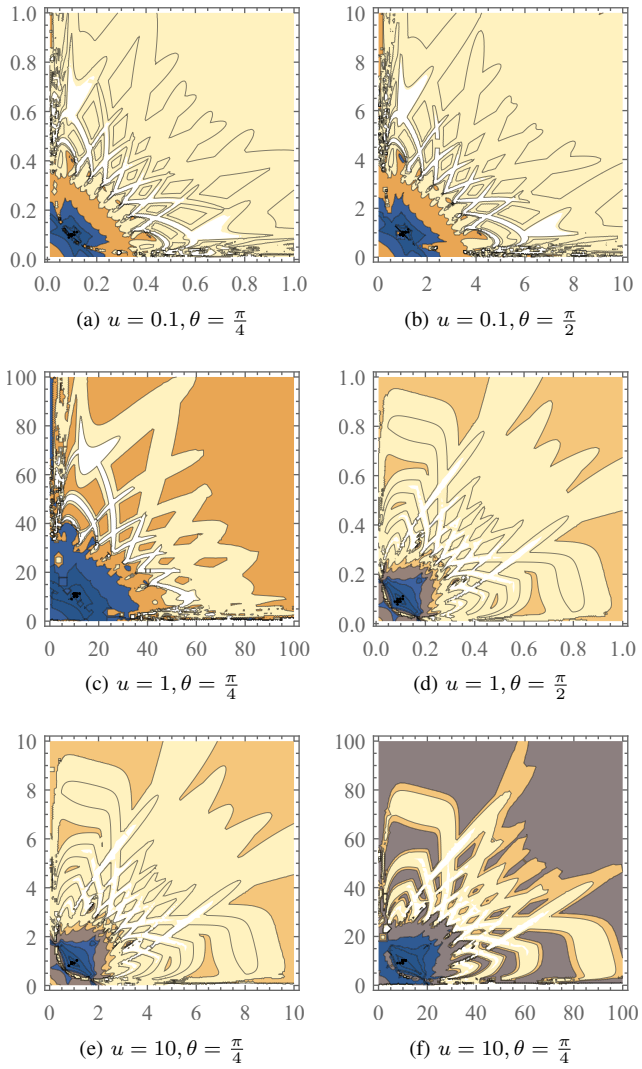

(a) $u = 0.1, \theta = \frac{\pi}{4}$ (b) $u = 0.1, \theta = \frac{\pi}{2}$

(c) $u = 1, \theta = \frac{\pi}{4}$ (d) $u = 1, \theta = \frac{\pi}{2}$

(e) $u = 10, \theta = \frac{\pi}{4}$ (f) $u = 10, \theta = \frac{\pi}{4}$

Fig. 1. $\epsilon_\kappa(\beta_1, \gamma_1)$ values in region $[0, 10u] \times [0, 10u]$ with $k = -0.05$. Arc length u is set to 0.1, 1, and 10 respectively with winding angles $\theta = \frac{\pi}{4}, \frac{\pi}{2}$. The black dots are evaluated points close to the minimum values within range $|\epsilon_\kappa - \min \epsilon_\kappa(\beta_1, \gamma_1)| \leqslant 0.05$.

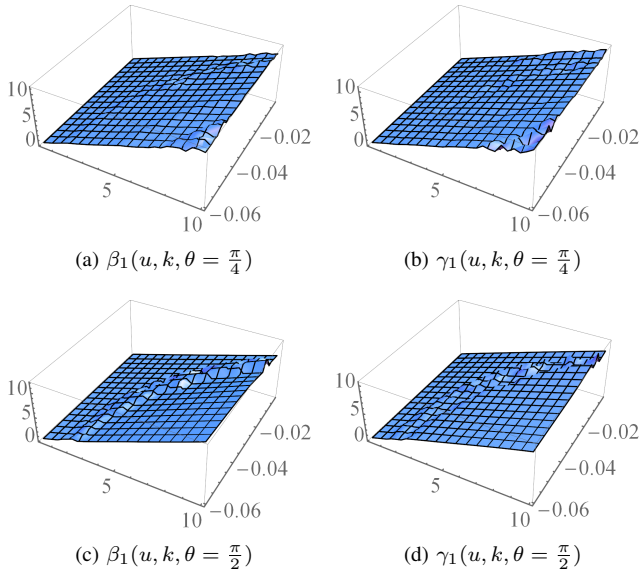

(a) $\beta_1(u, k, \theta = \frac{\pi}{4})$ (b) $\gamma_1(u, k, \theta = \frac{\pi}{4})$

(c) $\beta_1(u, k, \theta = \frac{\pi}{2})$ (d) $\gamma_1(u, k, \theta = \frac{\pi}{2})$

Fig. 2. Optimal β_1 and γ_1 values at each position (u, k) where $u \in [0, 10]$, $k \in [-0.06, 0]$ as θ is set to $\frac{\pi}{4}$ and $\frac{\pi}{2}$ respectively.

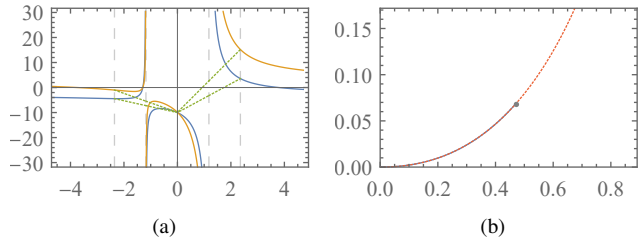

(a) (b)

Fig. 3. Divergence problem is shown by setting $\theta = \frac{\pi}{3}, u = 1$ and $k = -1.1\, k_d$: (a) Functions of $\beta_2(k)$ (blue solid) and $\gamma_2(k)$ (orange solid) have infinite values at $k = \pm k_d$ ($k_d = 1.1775$) with linear interpolations (green dashed) applied as $k \in (-2\, k_d, 2\, k_d)$. (b) Clothoid (red dashed) and its Bézier approximation (blue solid) using proposed method.

the irregular part. Alternatively, a similar search process is performed to locate the optimal position of $(\beta_1, \beta_2, \gamma_1, \gamma_2)$ by just considering the G^2 condition as described in [19]. Although smooth approximations can be always found with these methods, the property of G^3 continuity cannot be retained unfortunately. Here, we propose a new method to avoid the divergent positions as well as preserving the G^3 property by carefully adjusting the value of u. From (14) and $u > 0$, $\sigma > 0$, it can be found that $k < 0$. Thus only the negative divergent point $k = -k_d$ needs to be taken into consideration. Let $\xi_{0,k}, \xi_{1,k}$ be adjustable positive variables, and the divergent point and its neighborhood can be represented as $(-\xi_{0,k} k_d, -\xi_{1,k} k_d)$. So by specifying $k \in (-\infty, -\xi_{0,k} k_d] \cup [-\xi_{1,k} k_d, 0)$, or equivalently, $u \in (0, \frac{\xi_{1,k} k_d}{\sigma}] \cup [\frac{\xi_{0,k} k_d}{\sigma}, +\infty)$, we are able to guarantee G^3 continuity free of divergence problem. It is not a problem that the approximated Bézier curve has a shorter arc length than the original clothoid, because a lookup table formed afterwards with multiple elementary segments can be used to represent long enough clothoids.

III. Approximation of Basic Clothoid

Once all the shape parameters β_i and γ_i $(i = 1, 2)$ determined according to (10) and (16), any elementary clothoid $\mathbf{F}_\varepsilon(s)$ defined on $[0, u]$ with constraint (12) can be approximated with G^3 continuity. However, for those curves out of bounds, the above approximation procedure cannot be applied directly and appropriate preprocessing is needed. Taking a piece of clothoid with a positive initial curvature as an example, it may have a large sharpness which makes θ out of range easily as s increases. Elementary segments can only guarantee reasonable results when condition (12) is satisfied. Nevertheless, they are flexible to approximate a clothoid with arbitrary starting and ending curvatures κ_0, κ_1. By concatenating these elementary segments successively, a complete clothoid curve can be formed with curvature κ changing across the entire domain $(-\infty, +\infty)$ theoretically. In practice, we only need to focus on the half of this composed curve located in the first quadrant, and analyze a finite range consisting of N elementary segments in total. Let it be named the basic

clothoid and denoted by $\mathbf{F}_{\mathcal{L}}(s)$ with $\kappa \geqslant 0$ and $\sigma_{\mathcal{L}} = \sigma_{\varepsilon} > 0$. Also, the initial status is specified as $\kappa_{0,\mathcal{L}} = 0$ and $\theta_{0,\mathcal{L}} = 0$. Now considering the i-th piece among the first N elementary segments, $\mathbf{F}_{\varepsilon,i}(s)$ $(1 < i \leqslant N)$, its starting curvature $\kappa_{0,i}$ and winding angle $\theta_{0,i}$ should be equal to the ending values of the previous segment $\kappa_{1,i-1}$, $\theta_{1,i-1}$ respectively. Because σ_{ε} is set to be positive, $\kappa_{0,i}$ and $\theta_{0,i}$ becomes larger as i increases. On the other hand, the winding angle of an elementary segment has to be kept within the bound as well according to (12):

$$\theta = \kappa_0 u + \frac{\sigma_{\varepsilon}}{2} u^2 \leqslant \frac{\pi}{2}. \tag{18}$$

A. Arc Length Computation and Divergence Problem

Due to the constraint (18), the maximum allowable value of u is:

$$u_{\max} = \frac{1}{\sigma_{\varepsilon}} \left(\sqrt{\kappa_0^2 + 2\theta_{\max}\sigma_{\varepsilon}} - \kappa_0 \right), \tag{19}$$

where $\theta_{\max} \leqslant \frac{\pi}{2}$ is the maximum winding angle allowed, which is used to control the upper bound of the curvature error. For simplicity, $\theta_{\max}$ can be set to $\frac{\pi}{2}$, however, under certain circumstances it can be reduced to a smaller value if ϵ_{κ} is beyond an acceptable tolerance. In order to compute $\mathbf{F}_{\mathcal{L}}(s)$, arc lengths of all the elementary segment u_i $(i = 1, 2, \ldots)$ should be determined: they could be as close to 0 as possible but cannot be larger than $u_{\max}$. Typically, to approximate the basic clothoid of constant length, the maximum allowable value can be chosen as the arc length of each segment $u_i = u_{\max,i}$ to reduce the number of elementary pieces. On the other hand, splitting a curve into shorter segments often produces better approximation accuracy, thus in practice u_i should be carefully picked to balance computation efficiency with accuracy. In the case of $u_i = u_{\max,i}$, by combining (16), (17) and (19), the threshold of u_i is calculated as

$$u_{\tau} = \sqrt{\frac{2}{\sigma_{\varepsilon}}} \left(\theta_{\max}^2 - \sin^2(\theta_{\max}) \right)^{\frac{1}{4}}. \tag{20}$$

As a result, analysis of the divergence problem caused by k is equivalent to evaluating the relationship between u_i and u_{τ}: if they are close to each other, the value of u_i needs to be changed accordingly to satisfy G^3 continuity. Without loss of generality, by setting $u_i \in [0, u_{\max,i}]$, we obtain $\theta_{0,i} = \frac{1}{2}\sigma_{\varepsilon}\left(u_i^{\Sigma}\right)^2$ and $\kappa_{0,i} = \sigma_{\varepsilon} u_i^{\Sigma}$, where

$$u_i^{\Sigma} = \begin{cases} 0, & \text{if } i = 1, \\ \sum_{j=1}^{i-1} u_j, & \text{otherwise.} \end{cases} \tag{21}$$

Consequently, the i-th elementary segment $\mathbf{F}_{\varepsilon,i}(s)$ starting at point $(x_{0,i}, y_{0,i})^T$ can be derived by applying $\kappa_0 = \kappa_{0,i}$ in (4) and then transforming the acquired $\mathbf{F}_{\varepsilon}(s)$:

$$\mathbf{F}_{\varepsilon,i}(s) = \begin{pmatrix} x_{0,i} \\ y_{0,i} \end{pmatrix} + \mathbf{R}(\theta_{0,i})\, \mathbf{F}_{\varepsilon}(s), \quad t \in [0, u_i], \tag{22}$$

where $(x_{0,i}, y_{0,i})^T = \mathbf{F}_{\varepsilon,i-1}(u_{i-1})$ for $i > 1$ along with $(x_{0,1}, y_{0,1})^T = (0,0)^T$. In such a way, the basic curve $\mathbf{F}_{\mathcal{L}}(s)$ can be represented with a series of elementary pieces $\mathbf{F}_{\varepsilon,i}(s)$ $(i = 1, 2, \ldots, N)$, and each individual segment can be approximated with corresponding quintic Bézier curve $\mathbf{B}_{\varepsilon,i}(t) = (x_{0,i}, y_{0,i})^T + \mathbf{R}(\theta_{0,i})\mathbf{B}_{\varepsilon}(t)$ $(i = 1, 2, \ldots, N)$ effortlessly. More specifically, the curve $\mathbf{F}_{\mathcal{L}}(s)$ can be expressed as

$$\mathbf{F}_{\mathcal{L}}(s) = \sqrt{\frac{\pi}{\sigma_{\mathcal{L}}}} \begin{pmatrix} C\left(\sqrt{\frac{\sigma_{\mathcal{L}}}{\pi}} s\right) \\ S\left(\sqrt{\frac{\sigma_{\mathcal{L}}}{\pi}} s\right) \end{pmatrix}, \quad s \in [0, u_N^{\Sigma}]. \tag{23}$$

On these grounds, the approximation of a basic clothoid is computed offline and the total number of segments N can be arbitrarily large, although only a small number of segments are needed for practical use, especially when handling path design or smoothing problems. Algorithm 1 gives the procedure of approximating a basic clothoid with a successive generation of elementary curves by providing the sharpness $\sigma_{\mathcal{L}}$, number of segments N, and maximum winding angle $\theta_{\max} \in (0, \frac{\pi}{2}]$. The computed results can be stored in a lookup table for faster inquiries. The function $\textsc{Clothoid}\,(s, \kappa_0, \sigma, \theta_0, x_0, y_0)$ is computed according to equation (3), while the definition of $\textsc{Bézier}\,(t, u, \kappa_0, \sigma, \beta_1, \gamma_1, x_e, y_e)$ represents the final form of $\mathbf{B}_{\varepsilon}(t)$ (see Appendix A). In each loop, calculating coordinates of two endpoints of $\mathbf{F}_{\varepsilon,i}(s)$ $(i = 1, 2, \ldots, N)$ is necessary to formulate a quintic Bézier curve, which involves evaluation of Fresnel integrals. This process can be accomplished using numerical integration or any software with built-in functions supporting Fresnel integrals. From (19) and (20) we know that u_{τ} is always less than $u_{\max,1}$ and greater than a certain value when N is great enough seeing $\lim_{n\to\infty} u_{\max,n} = 0$, i.e., $\min_{i\in\mathbb{Z}^+} u_{\max,i} < u_{\tau} < \max_{i\in\mathbb{Z}^+} u_{\max,i}$ for any $\theta_{\max} \in (0, \frac{\pi}{2}]$. Therefore the divergence position is certainly included in the domain where both β_2 and γ_2 have abrupt changes. Previously we have already obtained a proper range of u in the form of $(0, \frac{\xi_{1,k} k_d}{\sigma}] \cup [\frac{\xi_{0,k} k_d}{\sigma}, +\infty)$ for u by analyzing the characteristic of k. Again, in consideration of the divergence problem, a ratio test of $u_{\max,i}$ to u_{τ} is used to quantify the closeness between $u_{\max,i}$ and u_{τ} for convenience. Values of $u_{\max,i}$ are restricted to $(0, \xi_u u_{\tau}]$, which corresponds to the left part $(0, \frac{\xi_{1,k} k_d}{\sigma}]$. By this means u_{τ} is always larger than $u_{\max,i}$ and G^3 continuity can be achieved for any valid inputs.

Algorithm 1 Approximate Basic Clothoid $\mathbf{F}_{\mathcal{L}}(s)$

function $\textsc{ApproxBasicClo}\,(\sigma_{\mathcal{L}}, N, \theta_{\max})$
1: $u_{\tau} \leftarrow \sqrt{2/\sigma_{\mathcal{L}}}(\theta_{\max}^2 - \sin^2(\theta_{\max}))^{\frac{1}{4}}$
2: **for** $i = 1$ to N **do**
3: **if** $i = 1$ **then**
4: $u_i^{\Sigma} \leftarrow 0$
5: **else**
6: $u_i^{\Sigma} \leftarrow \sum_{j=1}^{i-1} u_{\max,j}$
7: **end if**
8: $\kappa_{0,i} \leftarrow \sigma_{\mathcal{L}} u_i^{\Sigma}$
9: $u_{\max,i} \leftarrow (\sqrt{\kappa_{0,i}^2 + 2\theta_{\max}\sigma_{\mathcal{L}}} - \kappa_{0,i})/\sigma_{\mathcal{L}}$
10: **if** $u_{\max,i} > \xi_u u_{\tau}$ **then**
11: $u_{\max,i} \leftarrow \xi_u u_{\tau}$
12: **end if**
13: $(x_{0,i}, y_{0,i})^T \leftarrow \textsc{Clothoid}\,(u_i^{\Sigma}, 0, \sigma_{\mathcal{L}}, 0, 0, 0)$
14: $(x_{b,i}, y_{b,i})^T \leftarrow \textsc{Clothoid}\,(u_{\max,i}, \kappa_{0,i}, \sigma_{\mathcal{L}}, 0, 0, 0)$
15: $\mathbf{B}_{\varepsilon}(t) \leftarrow \textsc{Bézier}\,(t, u_{\max,i}, \kappa_{0,i}, \sigma_{\mathcal{L}}, u_{\max,i}, u_{\max,i}, x_{b,i}, y_{b,i})$

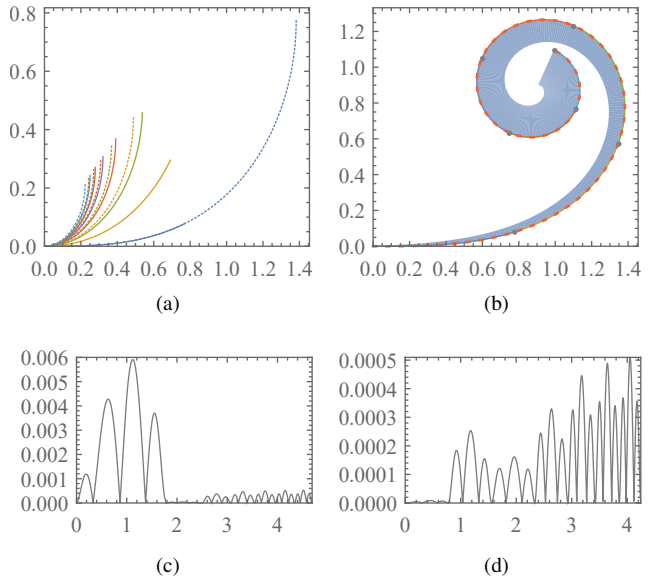

Fig. 4. Elementary segments used for basic clothoid approximation: (a) Individual Bézier curve $\mathbf{B}_{\varepsilon,i}$ $(i = 1, 2, \ldots, 7)$ are computed as primitives with setting $\theta_{\max} = \frac{\pi}{2}$, $N = 7$, and $\sigma_{\mathcal{L}} = 1$. It shows both the original segments (dashed) and modified ones after adjusting arc length (solid) by setting $\xi_u = 0.5$. (b) The basic clothoid $\mathbf{F}_{\mathcal{L}}(s)$ (dashed) and its Bézier approximation (solid) derived based on adjusted segments with the curvature magnitudes of the Bézier curves (shaded). (c) The upper bound of $\epsilon_\kappa(s)$ is greater than 0.005 before adjusting segment length. (d) $\epsilon_\kappa(s)$ is significantly reduced with maximum value less than 0.0005.

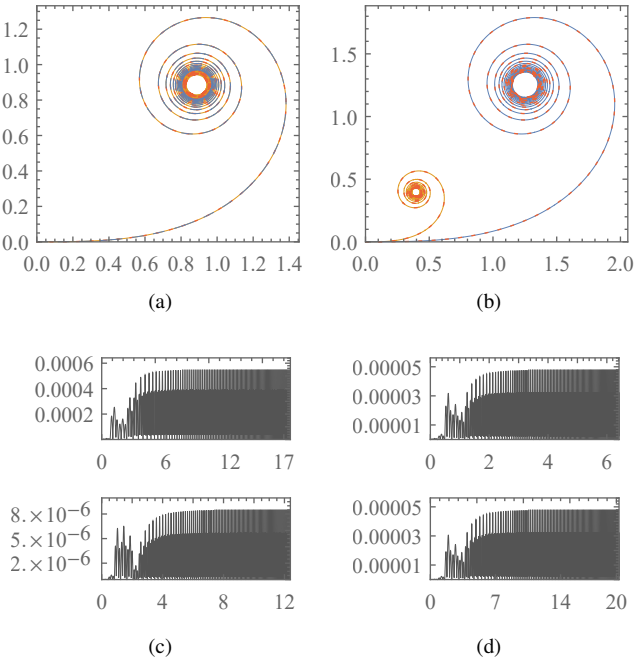

Fig. 5. Bézier approximations (solid) of basic clothoids (red dashed) and curvature error functions with different parameters: (a) $\theta_{\max} = \frac{\pi}{2}$ (blue) and $\theta_{\max} = \frac{\pi}{4}$ (orange) as $\sigma_{\mathcal{L}} = 1$. (b) $\sigma_{\mathcal{L}} = 0.5$ (blue) and $\sigma_{\mathcal{L}} = 5$ (orange) as $\theta_{\max} = \frac{\pi}{3}$. The corresponding error function $\epsilon_\kappa(s)$ of each approximation: (c) Top: $\theta_{\max} = \frac{\pi}{2}, \sigma_{\mathcal{L}} = 1$; Bottom: $\theta_{\max} = \frac{\pi}{4}, \sigma_{\mathcal{L}} = 1$; (d) Top: $\sigma_{\mathcal{L}} = 5, \theta_{\max} = \frac{\pi}{3}$; Bottom: $\sigma_{\mathcal{L}} = 0.5, \theta_{\max} = \frac{\pi}{3}$.

16: $\quad \mathbf{B}_{\varepsilon,i}(t) \leftarrow (x_{0,i}, y_{0,i})^T + \mathbf{R}(\sigma_{\mathcal{L}}(u_i^{\Sigma})^2/2)\, \mathbf{B}_{\varepsilon}(t)$
17: **end for**
18: **return** $(u_{\max,i})_{i=1}^N, (u_i^{\Sigma})_{i=1}^N, (\mathbf{B}_{\varepsilon,i}(t))_{i=1}^N$

B. Bézier Approximation and Error Analysis

An approximation of basic clothoid curve composed of $N = 7$ elementary segments is shown in Fig. 4. First, a series of Bézier curves $\mathbf{B}_{\varepsilon,i}(t)$ are computed as approximations of elementary clothoid segments $\mathbf{F}_{\varepsilon,i}(s)$. After proper linear transformations, they are joined up to form the approximated basic clothoid following Algorithm 1. The curvature magnitude of the Bézier approximation is also displayed with a shaded area, and it can be seen that both the curvature and its derivative with regard to arc length are continuous, which confirms the G^3 property (8) between adjacent segments. By adjusting the arc length $u_{\max,i}$ of each segment, the errors are significantly reduced.

In fact, $\epsilon_\kappa(s)$ is a piecewise function defined by multiple sub-functions $\epsilon_{\kappa,i}(s)$ $(i \in \mathbb{Z}^+)$, and each sub-function represents the curvature error between the elementary clothoid and its corresponding Bézier curve. For this reason, to analyze the upper bound of the error, we only need to evaluate the curvature error with regard to each pair of curves, i.e., $\mathbf{F}_{\varepsilon,i}(s)$ and $\mathbf{B}_{\varepsilon,i}(t)$. By applying G^3 conditions, both $\mathbf{F}_{\varepsilon,i}(s)$ and $\mathbf{B}_{\varepsilon,i}(t)$ can be alternatively represented with functions defined by a triplet $(\theta_{\max}, \sigma_{\mathcal{L}}, u_{\max,i})$. After arc length reparameterizations with regard to s, the obtained error function $\epsilon_\kappa(s)$ is only dependent on this triplet. Thus, there exists an infinite number of possible unique combinations since all these three parameters change continuously. Specifically, let's take the basic clothoid approximation with segment number $N = 100$ as a more practical example shown in Fig. 5. We start with considering the role of the first parameter $\theta_{\max}$ by setting the sharpness unchanged. As expected, longer Bézier curve can be formed with the growth of winding angle, however, the curvature error also becomes more significant. At the same time, it can be observed that the error function $\epsilon_\kappa(s)$ turns to be comparatively stable as the total arc length increases in all cases. More specifically, a relatively stable error range can be obtained by supplying a small enough value of $u_{\max,i}$. Similarly, to investigate the effect of sharpness $\sigma_{\mathcal{L}}$, we fix the other two parameters in the triplet. Though the approximated curves have significantly different arc lengths and shapes, the error functions are roughly within the same range as shown in Fig. 5d.

In consideration of the general case, Fig. 6 gives the numerical results of curvature errors evaluated at each position $(\theta_{\max}, \sigma_{\mathcal{L}}, u_{\max,i})$ within space $(0, \frac{\pi}{2}] \times (0, 10] \times (0, u_\tau)$, where the upper bound of $u_{\max,i}$ is determined by (20). It can be seen that $\theta_{\max}$ plays the most important role and larger error values appear where $\theta_{\max}$ is close to $\frac{\pi}{2}$. From Fig. 5 we already know that error variations are much more stable as $u_{\max,i}$ decreases. Thus we can ignore the effect of arc length change and focus on $\theta_{\max}$ and $\sigma_{\mathcal{L}}$ by choosing a small value of $u_{\max,i}$, as shown in Fig. 7. To further illustrate the point, Fig. 7a illustrates the results of $\epsilon_\kappa(\theta_{\max}, \sigma_{\mathcal{L}})$ evaluated at 2250 different positions within region $(0, \frac{\pi}{2}] \times (0, 10]$. The impact of one parameter can be examined by setting the other fixed as

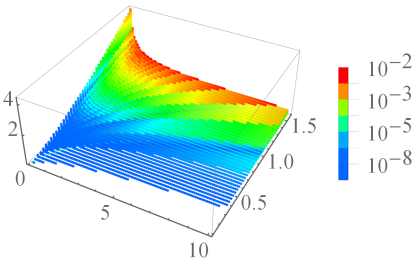

Fig. 6. Curvature error as a function of $\theta_{\max} \in (0, \frac{\pi}{2}], \sigma_{\mathcal{L}} \in (0, 10]$ and $u_{\max,i} \in (0, u_\tau)$: all the values of $\epsilon_\kappa(\theta_{\max}, \sigma_{\mathcal{L}}, u_{\max,i})$ are indicated by colors and within range $(0, 0.01)$.

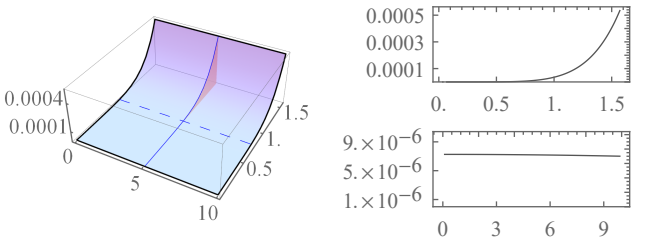

(a) (b)

Fig. 7. Curvature error with regard to $\theta_{\max}$ and $\sigma_{\mathcal{L}}$: (a) $\epsilon_\kappa(\theta_{\max}, \sigma_{\mathcal{L}})$ as $\theta_{\max} \in (0, \frac{\pi}{2}], \sigma_{\mathcal{L}} \in (0, 10]$ and $u_{\max,i} = 0.05$. (b) Top: $\epsilon_\kappa(\theta_{\max})$ as $\sigma_{\mathcal{L}} = 5.10$; Bottom: $\epsilon_\kappa(\sigma_{\mathcal{L}})$ as $\theta_{\max} = 0.77$.

shown in Fig. 7b. It can be seen that ϵ_κ is almost only relative to $\theta_{\max}$ and a smaller winding angle produces less error as expected. Also it demonstrates that the values of curvature error do not vary too much as $\sigma_{\mathcal{L}}$ changes. During creating a lookup table for a basic clothoid, this serves as a guidance that a smaller wingding angle $\theta_{\max}$ should be preferred when higher accuracy is required.

IV. General Clothoid Approximation

Revisiting the clothoid defined in (3), if both its sharpness and initial curvature are positive, the G^3 approximation can be made by reusing values of basic clothoid $\mathbf{F}_{\mathcal{L}}(s)$ in (23) due to the relationship:

$$\mathbf{F}(u) = \begin{pmatrix} x_0 \\ y_0 \end{pmatrix} + \mathbf{R}\left(\theta_0 - \frac{\kappa_0^2}{2\sigma}\right)\sqrt{\frac{\sigma_{\mathcal{L}}}{\sigma}}\left(\mathbf{F}_{\mathcal{L}}(s_u) - \mathbf{F}_{\mathcal{L}}(s_0)\right), \tag{24}$$

where $s_0 = \frac{\kappa_0}{\sqrt{\sigma\sigma_{\mathcal{L}}}}$ and $s_u = \frac{\kappa_0+\sigma u}{\sqrt{\sigma\sigma_{\mathcal{L}}}}$. In fact, a general clothoid curve with arbitrary sharpness and initial curvature can be approximated based on the basic clothoid curve approximation $(\mathbf{B}_{\varepsilon,i}(t))_{i=1}^N$ defined in the first quadrant, whose values are available in the existing lookup table. Algorithm 2 is implemented to locate the endpoint of a basic clothoid with arc length u in the lookup table, and the returned index l and parameter t facilitate the process of approximating a general clothoid. Function ArcLenPar is an implementation of the Hermite interpolation based algorithm mentioned earlier which takes a normalized arc length and a derivative of the given function as its input arguments. It generates a parameter $t \in [0, 1]$ at corresponding reference point with prescribed and normalized arc length, i.e., $u_n \in [0, 1]$.

Algorithm 2 Locate Endpoint in the Lookup Table

function LocateLUT $(\sigma_{\mathcal{L}}, N, \theta_{\max})$
1: $(u_{\max,i})_{i=1}^N, (u_i^\Sigma)_{i=1}^N, (\mathbf{B}_{\varepsilon,i}(t))_{i=1}^N \leftarrow$ ApproxBasicClo $(\sigma_{\mathcal{L}}, N)$
2: $i \leftarrow 1$
3: **while** $u_i^\Sigma \leqslant u$ **do**
4: $\quad i \leftarrow i + 1$
5: **end while**
6: $l \leftarrow i - 1$
7: $u_n \leftarrow (u - u_l^\Sigma)/u_{\max,l}$
8: $t \leftarrow$ ArcLenPar $(u_n, \mathbf{B}'_{\varepsilon,l}(t))$
9: **return** l, t

Let $\mathbf{B}(t)$ be the Bézier based approximation to the general clothoid (3), and the detailed process of constructing $\mathbf{B}(t)$ is illustrated in Algorithm 3. The strategy is first dividing the original curve into three different parts according to s_0, s_u, which are mapped to the existing lookup table subsequently. Then corresponding approximations are computed under different conditions: the starting and ending segments are approximated by a fragment of transformed quintic Bézier curve $\mathbf{B}_{\varepsilon,i}(t)$ respectively while the intermediate part is acquired by joining the remaining transformed pieces. Depending on the values of sharpness σ, initial curvature κ_0, and curve length u, parameters s_0 and s_u may appear in different quadrants. Thus corresponding transformation matrices are then applied to the basic clothoid approximation to place resulted curves in correct quadrant. Finally a group of polynomial functions established on the basis of standard quintic Bézier curves through linear transformations are obtained with their individual domains.

Algorithm 3 Approximate General Clothoid $\mathbf{F}(s)$

function GeneralClothoid $(u, \sigma, \kappa_0, \theta_0, (x_0, y_0)^T)$
1: $s_0, s_u \leftarrow \sqrt{|\sigma|/\sigma_{\mathcal{L}}}\kappa_0/\sigma, \sqrt{|\sigma|/\sigma_{\mathcal{L}}}(\kappa_0 + \sigma u)/\sigma$
2: $u_s, u_e \leftarrow |s_0|, |s_u|$
3: $l_s, t_s \leftarrow$ LocateLUT (u_s)
4: $l_e, t_e \leftarrow$ LocateLUT (u_e)
5: $(u_{\max,i})_{i=1}^N, (u_i^\Sigma)_{i=1}^N, (\mathbf{B}_{\varepsilon,i}(t))_{i=1}^N \leftarrow$ ApproxBasicClo $(\sigma_{\mathcal{L}}, N)$
6: $\mathbf{B}_0 \leftarrow \mathbf{B}_{\varepsilon,l_s}(t_s)$
7: $\mathbf{T} \leftarrow \mathbf{R}(\theta_0 - \kappa_0^2/(2\sigma))\sqrt{\sigma_{\mathcal{L}}/|\sigma|}\begin{pmatrix} 1 & 0 \\ 0 & \mathrm{sgn}(\sigma) \end{pmatrix}$
8: **if** $s_0 \geqslant 0, s_u \geqslant 0$ **then**
9: $\quad$ **if** $l_e - l_s = 0$ **then**
10: $\quad\quad I = ([t_s, t_e])$
11: $\quad$ **else**
12: $\quad\quad I = ([t_s, 1], [0, 1]_{\times(l_e - l_s - 1)}, [0, t_e])$
13: $\quad$ **end if**
14: $\quad$ **for** $l = l_s$ to l_e **do**
15: $\quad\quad \mathbf{B}(t) \leftarrow (x_0, y_0)^T + \mathbf{T}(\mathbf{B}_{\varepsilon,l}(t) - \mathbf{B}_0)$
16: $\quad$ **end for**
17: **else if** $s_0 < 0, s_u < 0$ **then**
18: $\quad$ **if** $l_s - l_e = 0$ **then**
19: $\quad\quad I = ([t_e, t_s])$
20: $\quad$ **else**
21: $\quad\quad I = ([0, t_s], [0, 1]_{\times(l_s - l_e - 1)}, [t_e, 1])$
22: $\quad$ **end if**

for $l = l_s$ to l_e **do**
  $\mathbf{B}(t) \leftarrow (x_0, y_0)^T - \mathbf{T}(\mathbf{B}_{\varepsilon,l}(t) - \mathbf{B}_0)$
end for
else
  $I = ([0, t_s], [0, 1]_{\times(l_e+l_s-2)}, [0, t_e])$
for $l = l_s$ to 1 **do**
  $\mathbf{B}(t) \leftarrow (x_0, y_0)^T - \mathbf{T}(\mathbf{B}_{\varepsilon,l}(t) - \mathbf{B}_0)$
end for
for $l = 1$ to l_e **do**
  $\mathbf{B}(t) \leftarrow (x_0, y_0)^T + \mathbf{T}(\mathbf{B}_{\varepsilon,l}(t) + \mathbf{B}_0)$
end for
end if
return $I, \mathbf{B}(t)$

As to the curvature error, it can be derived based on the error between the basic clothoid and its Bézier approximation. Because both translation and rotation cannot change the curve shape as well as the curvature, it can be expected that only the scale factor $\sqrt{\frac{\sigma_\mathcal{L}}{|\sigma|}}$ in Algorithm 3 determines the curvature error between approximated curve $\mathbf{B}(t)$ and the clothoid. Let $\epsilon_\kappa(s)$ be the curvature error function of $\mathbf{B}(t)$ and $\mathbf{F}(s)$ while $\epsilon_{\kappa,\mathcal{L}}(s_\mathcal{L})$ be the curvature error function of $\mathbf{F}_\mathcal{L}(s)$ and its Bézier approximation, and the following relation holds:

$$\epsilon_\kappa(s) = \sqrt{\frac{|\sigma|}{\sigma_\mathcal{L}}}\epsilon_{\kappa,\mathcal{L}}(s_\mathcal{L}), \tag{25}$$

where $s = \sqrt{\frac{\sigma_\mathcal{L}}{|\sigma|}}s_\mathcal{L}$. Thus to evaluate the curvature error (13) of a general Clothoid approximation, we can just refer to the curvature error $\epsilon_{\kappa,\mathcal{L}}(s_\mathcal{L})$ of the corresponding basic clothoid approximation and multiply it by a coefficient, i.e., the reciprocal of the scale factor.

V. Results and Discussion

We compare our newly proposed piecewise G^3 approximation method with existing algorithms including C^2 Hermite approximation via s-power series [16], G^3 Bézier approximation with numerical search in [18] and [19], and its improved variant "G^{2+}" deterministic approximation using linear interpolations [20]. For the sake of fairness, the functions used by all of these methods are set to be 5th order polynomials. The first comparison is made on a basic pair of Fresnel integrals $\mathbf{F}(s) = (C(s), S(s))^T$, which is equivalent to (3) by setting $\sigma = \pi, \kappa_0 = 0, \theta_0 = 0$ and $(x_0, y_0) = (0, 0)$. The approximation results using different approaches are shown in Fig. 8. The curvature error functions of corresponding approximations are demonstrated in Fig. 9. The C^2 method gives a mediocre result and has an acceptable error bound in this case. Benefiting from the numerical optimization procedure, it can be seen that the result of G^3 approximation is quite close to the original curve and the curvature error is satisfactory. For the "G^{2+}" method, since the corresponding k value falls within range $(-2\,k_d, 2\,k_d)$, adoption of linear interpolations free of complicated numerical computations is able to avoid the divergence problem, however, it potentially increased curvature errors as a trade-off and gives the worst approximation with only G^2 continuity ensured. Among all

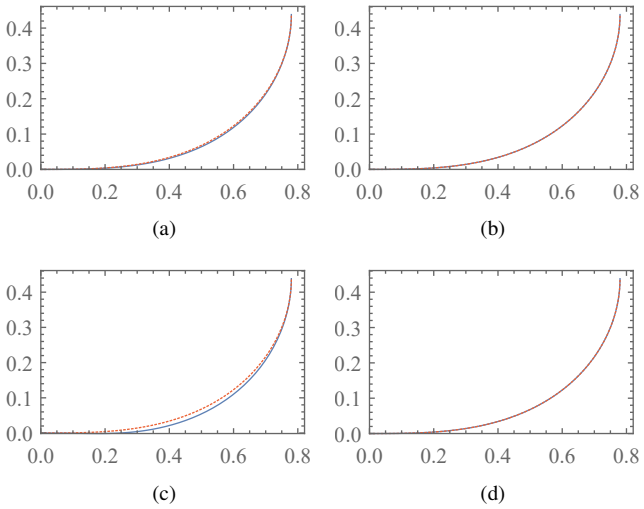

Fig. 8. Different approximations (blue solid) of $\mathbf{F}(s) = (C(s), S(s))^T$ (red dashed) of unit length: (a) C^2 Hermite approximation. (b) G^3 approximation with numerical search. (c) "G^{2+}" approximation. (d) Proposed G^3 approach.

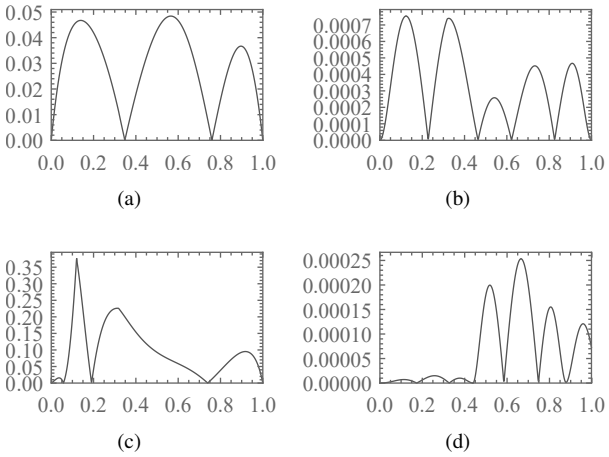

Fig. 9. $\epsilon_\kappa(s)$ of unit length clothoid approximations: (a) C^2 Hermite approximation. (b) G^3 approximation with numerical search. (c) "G^{2+}" approximation. (d) Proposed G^3 approach.

the results, the result based on the proposed method has the smallest curvature error and additionally, no numerical search procedure is involved. Moreover, it guarantees G^3 continuity over the entire domain. Here the basic clothoid used has specifications $\sigma_\mathcal{L} = 1$ and $\theta_{\max} = \frac{\pi}{2}$, and the curvature error can be reduced even further by specifying a smaller $\theta_{\max}$ as mentioned before.

Meanwhile, most available methods such as C^2, G^3, and G^{2+} approaches heavily rely on the normalization procedure during which the arc length of the clothoid is scaled. With the approximation computed based on the normalized curve, the final result is then obtained by rescaling the approximation curve back according to the same scale factor. Instead of scaling the clothoid, the proposed method is able to compute the approximation curve directly based on the lookup table. As an example of non-unit length clothoid approximation, Fig. 10 compares the approximation results of these methods with the

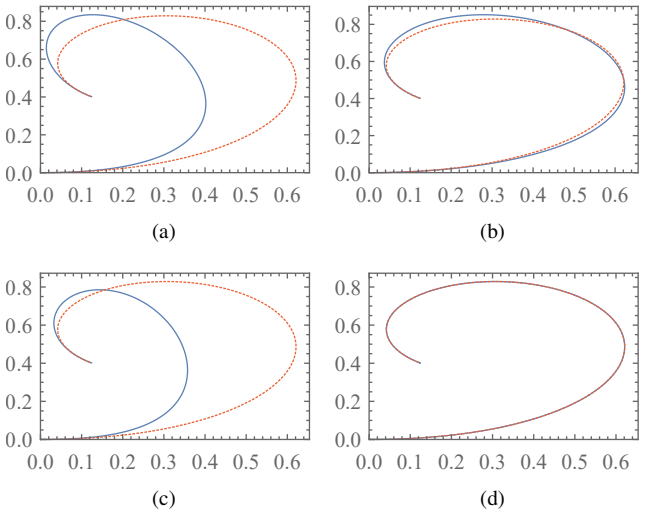

Fig. 10. Different approximations (blue solid) of $\mathbf{F}(s)$ (red dashed) with $s \in [0, 2]$: (a) C^2 Hermite approximation. (b) G^3 approximation with numerical search. (c) "G^{2+}" approximation. (d) Proposed G^3 approach.

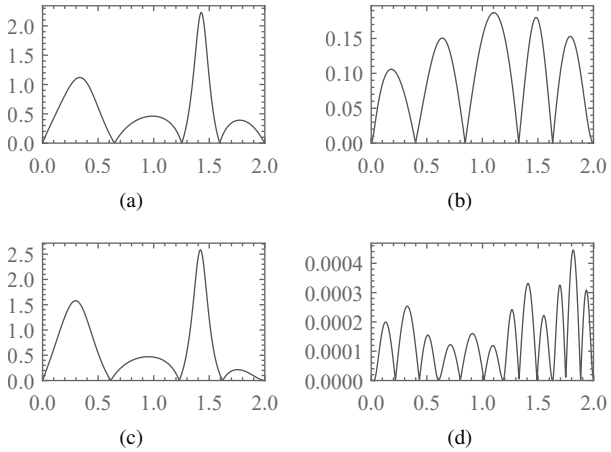

Fig. 11. $\epsilon_\kappa(s)$ of non-unit length clothoid approximations: (a) C^2 Hermite approximation. (b) G^3 approximation with numerical search. (c) "G^{2+}" approximation. (d) Proposed G^3 approach.

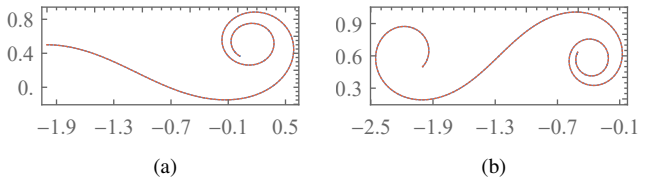

Fig. 12. Proposed G^3 approximations (blue solid) of $\mathbf{F}(s)$ (red dashed) with prescribed parameters: (a) $\sigma = 1.0$, $u = 6.0$, $\kappa_0 = -1.0$, $\theta_0 = 0.0$, $(x_0, y_0) = (-2.0, 0.5)$. (b) $\sigma = -2.0$, $u = 6.0$, $\kappa_0 = 5.0$, $\theta_0 = \frac{\pi}{4}$, $(x_0, y_0) = (-2.0, 0.5)$.

proposed approach by setting $(x_0, y_0) = (0, 0), \kappa_0 = 1, \theta_0 = 0$ and $\sigma = 1.8$. It can be observed that both C^2 and "G^{2+}" approximations have large deflections from the target clothoid curve though continuity constraints are satisfied at two ends. G^3 approximation curve has a better behavior but deflections still can be identified easily. Only the proposed method gives close approximation under this situation. In the sense of preserving curvatures, the proposed method also has the best performance as shown in Fig. 11 while other approximations lead to unacceptable results, i.e., $\epsilon_\kappa > 0.05$. In fact, the abnormal behaviors of the unsatisfactory results stem from the violating constraints that the winding angle of the scaled curve has to be limited within $[0, \frac{\pi}{2}]$ in those algorithms. As a consequence, only a small fraction of clothoid curves in (3) satisfy this criteria after scaling, thus these methods are not always applicable. It can be verified that the results of C^2, "G^{2+}", and G^3 approximations becomes even worse as the growth of arc length of approximated curve.

Apart from the previously mentioned problems, some methods have inherent disadvantages. For example, the G^3 method cannot handle the divergence problem properly thus the approximation curve does not exist if the clothoid curve meets certain criteria, e.g., $k = -k_d$. For longer curves with large curvature values, their winding angles are not able to meet the requirements after normalization. Thus these methods become impractical and cannot handle arbitrary case. Fig. 12 further demonstrates the flexibility and generality of our proposed method by giving two nontrivial examples of non-unit length clothoid curves with positive and negative sharpness values respectively, which are difficult to approximate within satisfactory error bounds using other methods.

Additionally, our method depends on clothoid parameters such as arc length and sharpness while explicit coordinates of the endpoints are not necessarily required, which can be especially useful when computing clothoid curves in path smoothing applications. We compare our method with the B-spline based algorithm presented in [28] with a specific example extracted from the same paper to illustrate the advantages of the proposed method for path smoothing. Without adding or removing waypoints, we use the Bézier based approximation of symmetric clothoid blending proposed in [29] and the resulted path is G^2 continuous, which can be reparameterized to satisfy C^2 continuity as the B-spline path. A comparison of two approaches is shown in Fig. 13 and the path curvature graph is obtained with regard to the normalized curve length. It can be seen that due to the inherent advantages of clothoid, the smoothed path using proposed method has a lower curvature bound, and its total length is also slightly shorter than the B-spline result. Thus the Bézier based path is less sharper compared with the B-spline path, and it implies that the latter path is more difficult to follow and requires a larger steering angle, which is only valid for vehicles with higher maneuverability.

VI. Conclusion

This paper presents a smooth approximation method of clothoid on the basis of quintic Bézier curves. On the basis of a lookup table computed offline, any kinds of clothoid curves can be approximated efficiently without numerical optimization procedures. By restricting the winding angle within a limited range, the error can be bounded to an acceptable tolerance, while the analysis shows that the approximation accuracy can be further improved by adjusting the winding angle. Also

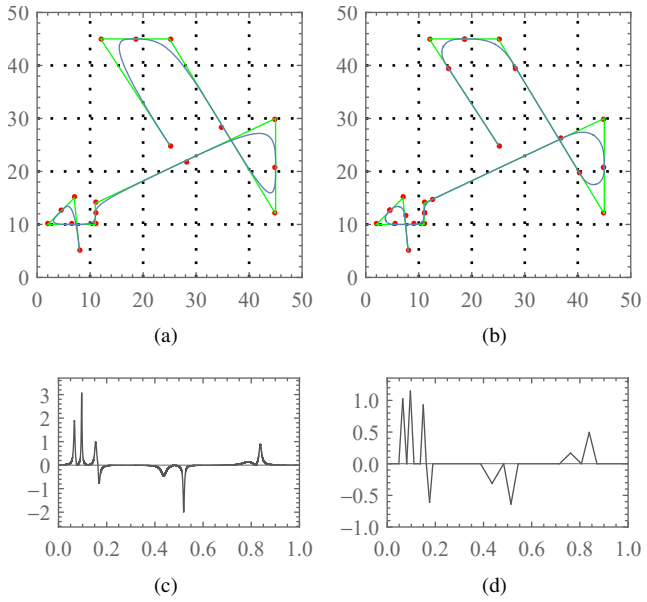

Fig. 13. Path smoothing example with given waypoints: (a) B-spline smoothing. (b) Bézier based smoothing. (c) Curvature profile of B-spline path. (d) Curvature profile of Bézier based path.

this method is robust and can always guarantee G^3 continuity even under the divergent conditions. The effectiveness of the approximation method is explained through comparing with existing approaches and its applicability in path smoothing applications is also demonstrated.

Furthermore, the method proposed here can also be used in road design and other applications where clothoids are involved. Though only approximation of clothoid curve is addressed in this research, further work will consider the feasibility of extending this method to general Cornu spirals. Also, by combining geometric approach with sampling or search based path planning algorithms, real time path planning frameworks directly based on the Bézier approximation are expected to be implemented.

APPENDIX A

Bézier curve $\text{BÉZIER}\,(t, u, \kappa_0, \sigma, \beta_1, \gamma_1, x_e, y_e)$ satisfying G^3 continuity can be obtained by substituting relationship (10) into the following function:

$$\mathbf{Q}\,(t, u, \kappa_0, \sigma, \beta_1, \gamma_1, \beta_2, \gamma_2, x_b, y_b) = \begin{pmatrix} Q_x \\ Q_y \end{pmatrix},$$

where x_b and y_b are the coordinates of the second endpoint of the clothoid curve and

$$\begin{aligned} Q_x =& \frac{1}{2}t(2t^4x_b - 2t^3(t-1)(5x_b - \gamma_1\cos(\frac{1}{2}u(2\kappa_0+\sigma u))) \\ &+ t^2(t-1)^2(20x_b + \gamma_1^2(\kappa_0+\sigma u)(-\sin(\frac{1}{2}u(2\kappa_0 \\ &+ \sigma u))) + (\gamma_2 - 8\gamma_1)\cos(\frac{1}{2}u(2\kappa_0+\sigma u))) \\ &+ 2\beta_1(t-1)^4 - (8\beta_1+\beta_2)t(t-1)^3), \end{aligned}$$

$$\begin{aligned} Q_y =& \frac{1}{2}t^2(2t^3y_b - 2t^2(t-1)(5y_b - \gamma_1\sin(\frac{1}{2}u(2\kappa_0+\sigma u))) \\ &+ t(t-1)^2(20y_b + (\gamma_2 - 8\gamma_1)\sin(\frac{1}{2}u(2\kappa_0+\sigma u)) \\ &+ \gamma_1^2(\kappa_0+\sigma u)\cos(\frac{1}{2}u(2\kappa_0+\sigma u))) - \beta_1^2\kappa_0(t-1)^3). \end{aligned}$$

REFERENCES

[1] S. M. LaValle, *Planning algorithms*. Cambridge university press, 2006.

[2] A. Scheuer and T. Fraichard, "Continuous-curvature path planning for car-like vehicles," in *Intelligent Robots and Systems, 1997. IROS'97., Proceedings of the 1997 IEEE/RSJ International Conference on*, vol. 2. IEEE, 1997, pp. 997–1003.

[3] P. Soueres and J.-D. Boissonnat, "Optimal trajectories for nonholonomic mobile robots," in *Robot motion planning and control*. Springer, 1998, pp. 93–170.

[4] D. Walton and D. Meek, "Computer-aided design for horizontal alignment," *Journal of transportation engineering*, vol. 115, no. 4, pp. 411–424, 1989.

[5] T. Fraichard and A. Scheuer, "From reeds and shepp's to continuous-curvature paths," *Robotics, IEEE Transactions on*, vol. 20, no. 6, pp. 1025–1035, 2004.

[6] J.-w. Choi, R. Curry, and G. Elkaim, "Path planning based on bézier curve for autonomous ground vehicles," in *World Congress on Engineering and Computer Science 2008, WCECS'08. Advances in Electrical and Electronics Engineering-IAENG Special Edition of the*. IEEE, 2008, pp. 158–166.

[7] C. Chen, Y. He, C. Bu, J. Han, and X. Zhang, "Quartic bézier curve based trajectory generation for autonomous vehicles with curvature and velocity constraints," in *Robotics and Automation (ICRA), 2014 IEEE International Conference on*. IEEE, 2014, pp. 6108–6113.

[8] A. Neto, D. G. Macharet, M. F. Campos *et al.*, "Feasible rrt-based path planning using seventh order bézier curves," in *Intelligent Robots and Systems (IROS), 2010 IEEE/RSJ International Conference on*. IEEE, 2010, pp. 1445–1450.

[9] A. M. Lekkas, A. R. Dahl, M. Breivik, and T. I. Fossen, "Continuous-curvature path generation using fermat's spiral," *Modeling, Identification and Control*, vol. 34, no. 4, p. 183, 2013.

[10] H. Bruyninckx and D. Reynaerts, "Path planning for mobile and hyper-redundant robots using pythagorean hodograph curves," in *Advanced Robotics, 1997. ICAR'97. Proceedings., 8th International Conference on*. IEEE, 1997, pp. 595–600.

[11] M. Brezak and I. Petrovic, "Real-time approximation of clothoids with bounded error for path planning applications," *Robotics, IEEE Transactions on*, vol. 30, no. 2, pp. 507–515, 2014.

[12] K. D. Mielenz, "Computation of fresnel integrals," *JOURNAL OF RESEARCH-NATIONAL INSTITUTE OF STANDARDS AND TECHNOLOGY*, vol. 102, pp. 363–366, 1997.

[13] ——, "Computation of fresnel integrals. ii," *Journal of Research of the National Institute of Standards and Technology*, vol. 105, no. 4, pp. 589–590, 2000.

[14] L. Z. Wang, K. T. Miura, E. Nakamae, T. Yamamoto, and T. J. Wang, "An approximation approach of the clothoid curve defined in the interval [0, π/2] and its offset by free-form curves," *Computer-Aided Design*, vol. 33, no. 14, pp. 1049–1058, 2001.

[15] J. Sánchez-Reyes, "Applications of the polynomial s-power basis in geometry processing," *ACM Transactions on Graphics (TOG)*, vol. 19, no. 1, pp. 27–55, 2000.

[16] J. Sánchez-Reyes and J. M. Chacón, "Polynomial approximation to clothoids via s-power series," *Computer-Aided Design*, vol. 35, no. 14, pp. 1305–1313, 2003.

[17] R. Cripps, M. Hussain, and S. Zhu, "Smooth polynomial approximation of spiral arcs," *Journal of computational and applied mathematics*, vol. 233, no. 9, pp. 2227–2234, 2010.

[18] B. Cross and R. J. Cripps, "G3 quintic polynomial approximation for generalised cornu spiral segments," *Journal of Computational and Applied Mathematics*, vol. 236, no. 13, pp. 3111–3122, 2012.

[19] L. Lu, "A note on quintic polynomial approximation of generalized cornu spiral segments," *Journal of Computational and Applied Mathematics*, vol. 253, pp. 123–130, 2013.

[20] B. Cross and R. J. Cripps, "Efficient robust approximation of the generalised cornu spiral," *Journal of Computational and Applied Mathematics*, vol. 273, pp. 1–12, 2015.

[21] A. Nutbourne, P. McLellan, and R. Kensit, "Curvature profiles for plane curves," *Computer-aided design*, vol. 4, no. 4, pp. 176–184, 1972.

[22] M. Abramowitz, I. A. Stegun *et al.*, *Handbook of mathematical functions*. Dover New York, 1965, vol. 1046.
[23] B. A. Barsky and T. D. DeRose, "Geometric continuity of parametric curves: three equivalent characterizations," *IEEE Computer Graphics and Applications*, no. 6, pp. 60–68, 1989.
[24] M. Madi, "Closed-form expressions for the approximation of arclength parameterization for bezier curves," *International journal of applied mathematics and computer science*, vol. 14, no. 1, pp. 33–42, 2004.
[25] V. Hernández-Mederos and J. Estrada-Sarlabous, "Sampling points on regular parametric curves with control of their distribution," *Computer Aided Geometric Design*, vol. 20, no. 6, pp. 363–382, 2003.
[26] J. M. Ali, R. Tookey, J. Ball, and A. Ball, "The generalised cornu spiral and its application to span generation," *Journal of Computational and Applied Mathematics*, vol. 102, no. 1, pp. 37–47, 1999.
[27] J. A. Nelder and R. Mead, "A simplex method for function minimization," *The computer journal*, vol. 7, no. 4, pp. 308–313, 1965.
[28] M. Elbanhawi, M. Simic, and R. N. Jazar, "Continuous path smoothing for car-like robots using b-spline curves," *Journal of Intelligent & Robotic Systems*, pp. 1–34, 2015.
[29] D. J. Walton and D. S. Meek, "A controlled clothoid spline," *Computers & Graphics*, vol. 29, no. 3, pp. 353–363, 2005.